Wolfgang E. Nagel
Dietmar H. Kröner
Michael M. Resch *Editors*

High Performance Computing in Science and Engineering '18

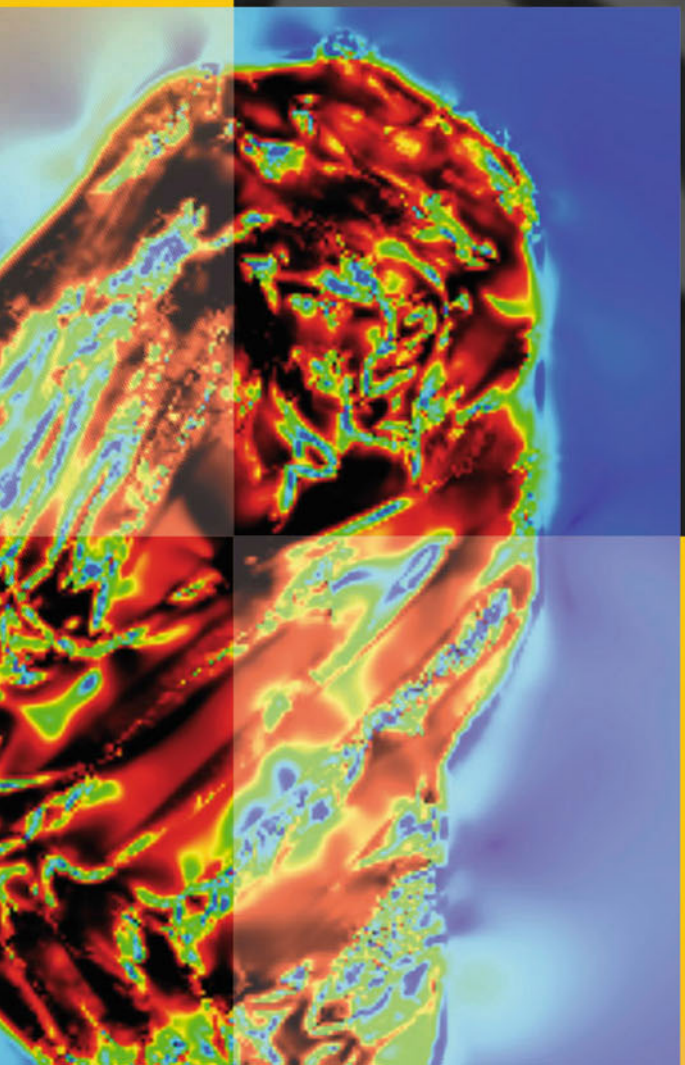

H L R S

Springer

High Performance Computing in Science and Engineering ’18

Wolfgang E. Nagel · Dietmar H. Kröner ·
Michael M. Resch
Editors

High Performance Computing in Science and Engineering ’18

Transactions of the High Performance Computing Center, Stuttgart (HLRS) 2018

Springer

Editors
Wolfgang E. Nagel
Zentrum für Informationsdienste und
Hochleistungsrechnen (ZIH)
Technische Universität Dresden
Dresden, Germany

Dietmar H. Kröner
Abteilung für Angewandte Mathematik
Universität Freiburg
Freiburg, Germany

Michael M. Resch
Höchstleistungsrechenzentrum Stuttgart
(HLRS)
Universität Stuttgart
Stuttgart, Germany

Front cover figure: Stress distribution in a section of a dual-phase steel after quenching predicted by a multiphase-field simulation. The martensitic transformation leads both to high stresses in the former austenitic islands and to a considerable stress input into the surrounding ferritic matrix. Details can be found in "Multiphase-Field Modeling and Simulation of Martensitic Phase Transformation in Heterogeneous Materials" by E. Schoof, C. Herrmann, D. Schneider, J. Hötzer, and B. Nestler, Institute of Applied Materials, Karlsruhe Institute of Technology (KIT), Germany and Institute of Digital Materials Science, Karlsruhe University of Applied Sciences, Germany, on page 475 ff.

ISBN 978-3-030-13324-5 ISBN 978-3-030-13325-2 (eBook)
https://doi.org/10.1007/978-3-030-13325-2

Library of Congress Control Number: 2019932797

Mathematics Subject Classification (2010): 65Cxx, 65C99, 68U20, 90-08, 97M50

This Springer imprint is published by the registered company Springer Nature Switzerland AG
The registered company address is: Gewerbestrasse 11, 6330 Cham, Switzerland

Contents

Part VII Miscellaneous Topics

Part I
Physics

In this section, six physics projects are described, which achieved important scientific results in 2017/18 by using Hazel Hen at the HLRS and ForHLR II of the Steinbuch Center.

Fascinating new results are being presented in the following pages on astrophysical systems (simulations of galaxy formation, neutron star and binary merger evolutions, and of photoionization and radiative charge transfer), soft matter systems (interaction between blood proteins and nanoparticles), many body quantum systems (simulations of trapped ultracold quantum systems) and high energy physics systems (simulations of the QCD phase diagram on the lattice).

The studies of the astrophysical systems have focused on galaxy formation, neutron star and binary merger evolutions, and on photoionization and radiative charge transfer of several particles.

D. Nelson, A. Pillepich, V. Springel, R. Pakmor, L. Hernquist, R. Weinberger, S. Genel, M. Vogelsberger, F. Marinacci, P. Torrey, J. Naiman from Garching (D.N., V.S.,), Heidelberg (A.P., V.S., R.P., R.W.), Cambridge USA (L.H., J.N., M.V., F.M., P.T.), and New York (S.G.), present in their project *GCS-DWAR* results from the TNG50 run, the third and final volume of the cosmological, magnetohydrodynamical simulations in the IllustrisTNG project (AREPO code), with over 20 billion resolution elements and a spatial resolution of 100 parsecs. The authors conclude that the results of the TNG50 run has been successful for the analysis of many observational data, e.g., the star formation histories and abundances of dwarf galaxies in the first few billion years, the detailed mapping of our Galaxy's stellar system, the imaging and spectroscopic characterisation of the galaxy populations residing in nearby galaxy clusters like Virgo, Fornax, and Coma, the X-ray maps of the outskirts of galaxy clusters, integral-field spectroscopy campaigns of nearby galaxies, the characterisation of circumgalactic and IGM gas, and magnetic field measurements in halos and in the disks of galaxies.

L. Rezolla, F. Guercilena, and E. Most from the University of Frankfurt investigated in their project *HypeBBHs* interesting phenomena of neutron stars and black holes, as well of mergers, by numerically solving the Einstein equations for spacetime evolution and the equations of hydrodynamics and magnetohydrodynamics, using a variety of codes, e.g. the open-source McLachlan code, self-developed codes (WhiskeyTHC, WhiskeyMHD, WhiskeyResitive), and the FIL code, an extension

of the open-source code IllinoisGRMHD. The focus of the project is on the general behaviour of black hole systems in vacuum, the study of rigidly and differentially rotating isolated neutron stars, the evolution of neutron stars and accretion disks systems, the evolution and properties of magnetized neutron stars in the contexts of both ideal and resistive magnetohydrodynamics, and on the study of ejecta in binary neutron star systems and the resulting implications for nucleosynthesis. A new approach to relativistic hydrodynamics has been developed, the accuracy of numerical waveforms from binary mergers has been investigated, as well as the nucleosynthesis in the ejecta of binary neutron star mergers.

B. M. McLaughlin, C. P. Ballance, M. S. Pindzola, P. C. Stancil, J.F. Babb, S. Schippers and A. Müller from the Universities of Belfast (B.M.M., C.P.B.), Auburn (M.S.P.), Georgia (P.C.S.), Cambridge USA (J.F.B.), and Giessen (S.S., A.M.) investigated in their project *PAMOP2* atomic, molecular and optical collisions on petaflop machines, relevant for astrophysical applications, for magnetically-confined fusion and plasma modeling, and as theoretical support for experiments and satellite observations. The Schrödinger and Dirac equations have been solved with the R-matrix or R-matrix with pseudo-states approach, and the time dependent close-coupling method has been used. Various systems and phenomena have been investigated, in detail the photoionisation of calcium ions and of zinc ions, the electron impact excitation of molybdenum, the electron impact double ionization of the H_2 molecule, the X-ray emission in collisions of O^{8+} ions with H and He atoms, the radiative charge transfer of He^+ ions with Ar atoms, and the radiative association of Si and O atoms and of C and S atoms.

Studies of the soft matter systems have focused on the interaction of blood proteins with nanoparticles.

T. Schäfer, C. Muhl, M. Barz, F. Schmid and G. Settanni from the University of Mainz investigated in their project *Flexadfg* interaction of blood proteins with nanoparticles by Molecular Dynamics simulations, using the program NAMD and CHARMM force fields, a cell-list algorithm, and a smooth particle mesh Ewald (PME) method, and in selected cases a "Hamiltonian replica exchange with solute tempering" (REST2) sampling technique. One of the project goals was to identify the features that make a polymer amenable for coating nanoparticles for drug delivery, with particular focus on salt dependent behaviour of poly(ethylene glycol) (PEG). The simulations helped to explain how PEG chains shrink in the presence of potassium ions and they are being used to reveal how PEG and PSAR show similar stealth effects. In addition, interactions of blood proteins with silica has been explored.

In the last granting period, quantum mechanical properties of high energy physics systems have been investigated as well as the quantum many body dynamics of trapped bosonic systems.

S. Borsanyi, Z. Fodor, J. Günther, S. D. Katz, A. Pasztor, I. P. Vazquez, C. Ratti, and K. K. Szabó from Wuppertal (S.B., Z.F., A.P., K.K.S.), Budapest (Z.F., S.D.K., J.G., S.D.K.), the FZ Jülich (Z.F., K.K.S.), Regensburg (J.G., S.D.K.) and Houston (I.P.V., C.R.) studied in their project *GCS-POSR* the QCD phase diagram from the lattice. In the project, several diagonal and non-diagonal fluctuations of conserved charges have been computed in a system of 2+1+1 quark flavors with physical masses, on a

lattice with size $48^3 \times 12$. From high statistics lattice QCD simulations several μ_B-derivatives of observables have been computed, which account for the confinement-deconfinement transition between the hadron gas and quark gluon plasma phases. Higher order fluctuations at $\mu_B = 0$ were obtained as derivatives of the lower order ones. From these correlations and fluctuations ratios of net-baryon number cumulants have been constructed as functions of temperature and chemical potential, satisfying important experimental conditions. In addition, in the project fluctuations were computed from a simple model, assuming the absence of a nearby critical end point in the phase diagram, and good agreement with the simulation results was found. Based on their findings, the authors conclude that the experimental finding of a critical end-point below $\mu_B/T < 2$ is unlikely.

O.E. Alon, R. Beinke, C. Bruder, L.S. Cederbaum, S. Klaiman, A.U.J. Lode, K. Sakman, M. Theisen, M.C. Tsatsos, S.E. Weiner, and A.I. Streltsov from the Universities of Haifa (O.E.A.), Heidelberg (R.B., L.S.C., S.K., M.T., A.I.S.), Basel (C.B., A.U.J.L.), Wien (K.S.), Sao Paulo (M.C.T.), and Berkeley (A.S.) studied in their project *MCTDHB* trapped ultracold atomic systems by their method termed multi-configurational time-dependent Hartree for bosons (MCTDHB and MCTDH-X software packages). The principal investigators investigated entropies and correlations of ultracold bosons in a lattice, crystallization of bosons with dipole-dipole interactions and its detection in single-shot images, studied the management of correlations in ultracold gases, explored the pulverising of a Bose-Einstein-Condensate (BEC), the dynamical pulsation of ultracold droplet crystals by laser light, two-component bosons interacting with photons in a cavity, analysed the impact of the range of the interaction on the quantum dynamics of a bosonic Josephson junction, computed the exact many-body wavefunction and properties of trapped bosons in the infinite-particle limit, analyzed the angular-momentum conservation in a BEC, investigated the variance of an anisotropic BEC and enhanced many-body effects in the excitation spectrum of a weakly-interacting rotating BEC.

Peter Nielaba
Fachbereich Physik, Universität Konstanz
78457 Konstanz, Germany
e-mail: peter.nielaba@uni-konstanz.de

The TNG50 Simulation of the IllustrisTNG Project: Bridging the Gap Between Large Cosmological Volumes and Resolved Galaxies

Dylan Nelson, Annalisa Pillepich, Volker Springel, Rüdiger Pakmor, Lars Hernquist, Rainer Weinberger, Shy Genel, Mark Vogelsberger, Federico Marinacci , Paul Torrey and Jill Naiman

Abstract Cosmological hydrodynamical simulations of galaxy formation are a powerful theoretical tool, and enable us to directly calculate the observable signatures resulting from the complex process of cosmic structure formation. Here we present early results from the ongoing TNG50 run, an unprecedented 'next generation' cosmological, magnetohydrodynamical simulation—the third and final volume of the IllustrisTNG project, with over 20 billion resolution elements and capturing spatial scales of ∼100 parsecs. It incorporates the comprehensive TNG model for galaxy formation physics, and we here describe the simulation scope, novel achievements, and early investigations on resolved galactic and halo structural properties.

D. Nelson (✉) · V. Springel
Max-Planck-Institut für Astrophysik, Karl-Schwarzschild-Str. 1, 85741 Garching, Germany
e-mail: dnelson@mpa-garching.mpg.de

V. Springel
e-mail: volker.springel@h-its.org

A. Pillepich
Max-Planck-Institut für Astronomie, Königstuhl 17, 69117 Heidelberg, Germany
e-mail: pillepich@mpia-hd.mpg.de

V. Springel · R. Pakmor · R. Weinberger
Heidelberg Institute for Theoretical Studies, Schloss-Wolfsbrunnenweg 35,
69118 Heidelberg, Germany
e-mail: ruediger.pakmor@h-its.org

R. Weinberger
e-mail: rainer.weinberger@h-its.org

V. Springel
Zentrum für Astronomie der Universität Heidelberg, ARI, Mönchhofstr. 12,
69120 Heidelberg, Germany

W. E. Nagel et al. (eds.), *High Performance Computing in Science and Engineering '18*, https://doi.org/10.1007/978-3-030-13325-2_1

1 Introduction

Observed galaxies today range in mass from a few thousand to a few trillion times the mass of the sun, range in physical size from a fraction to tens of kilo-parsecs, and span a wide variety of morphologies, from ultra-diffuse extended disks to ultra-compact spheroidal nuggets. Galaxies can exist in isolation, or as members of rich clusters—one out of thousands. Throughout space their distribution traces a filamentary cosmic web of matter which has arisen from 13.8 billion years of cosmic evolution, starting from the nearly homogeneous distribution of matter in the early universe. According to the current paradigm this large-scale structure is driven by the dominant presence of cold dark matter (CDM), which results in a hierarchical growth governing the formation and transformation of galaxies.

The mathematical equations governing the dominant physical processes are non-linear, complex, and highly coupled. As a result, computational methods are an absolute requirement for their solution, although the inherently multi-scale, multi-physics nature of the problem poses significant challenges. Numerical simulations of the formation and evolution of galaxies in the full cosmological context of our evolving universe have reached impressive levels of sophistication, achieving along the way a number of notable successes as well as failures. Early, pioneering beginnings with dark-matter only simulations over the past thirty years [1–3] paved the way for keystone projects of the past decade [4, 5]. These DM-only simulations do not, however, provide direct predictions for the *observable* properties of galaxies, and additional modeling is required to make any firm connection to observational data. To do so, it has recently become possible to simultaneously model, in addition to gravity, the hydrodynamics of cosmic gas (i.e., CFD of relatively diffuse plasmas) together with the principal baryonic physics of relevance. More accurate fluid codes are coupled to increasingly sophisticated physical models, which are then used to

L. Hernquist · J. Naiman
Harvard-Smithsonian Center for Astrophysics, 60 Garden Street, Cambridge, MA 02138, USA
e-mail: lars@cfa.harvard.edu

S. Genel
Center for Computational Astrophysics, 162 Fifth Avenue, Flatiron, New York 10010, USA
e-mail: shygenelastro@gmail.com

M. Vogelsberger · F. Marinacci · P. Torrey
Department of Physics, MIT Kavli Institute for Astrophysics and Space Research, Massachusetts Institute of Technology, Cambridge, MA 02139, USA
e-mail: mvogelsb@mit.edu

F. Marinacci
e-mail: fmarinac@mit.edu

execute simulations of ever increasing scope. Theoretically, these calculations yield a self-consistent and uniquely predictive realization of a given cosmological model.

Large volumes allow statistically robust comparisons of entire populations of galaxies—we no longer are relegated to simulating single objects. Cosmological hydrodynamical simulations have emerged as powerfully predictive theoretical models, and this recent development has been made clear with the Illustris [6–9] and EAGLE [10, 11] simulations. Together with other cosmological simulations [12, 13] these projects have finally succeeding in demonstrating that hydrodynamical simulations of structure formation, run at kilo-parsec spatial resolutions, can reasonably reproduce a number of fundamental scaling relations and properties of observed galaxy populations. This zeroth order agreement has buttressed many theoretical investigations and predictions. At the same time, however, it has revealed many telling shortcomings in the current generation of models.

IllustrisTNG is a 'next generation' series of large, cosmological, gravo-magneto-hydrodynamical simulations incorporating a comprehensive model for galaxy formation physics. Conducted over the past two years on the Hazel Hen machine at the High Performance Computing Center Stuttgart (HLRS) and supported by two Gauss Centre for Supercomputing allocations (GCS-ILLU in 2014, and GCS-DWAR in 2016) it includes three main runs: TNG50, TNG100, and TNG300. The latter two have been completed and recently presented [14–18]. TNG50 is the most computational demanding of the three simulations by far: with an anticipated cost of $\sim$100 M core hours the simulation is still ongoing, and we present herein early results from this project.

2 IllustrisTNG: Physical and Numerical Developments

The IllustrisTNG simulation project[1] expands upon the original Illustris simulation in two principal aspects. First, it alleviates the major problems—that is, model deficiencies [19]—with respect to strongly constraining low redshift observations. Second, it significantly expands upon the original scope, with simulations of larger volumes, at higher resolution, and with new physics.

2.1 The TNG Galaxy Formation Model

In terms of physical modeling, we retain the same basic approach as in Illustris, acknowledging that physics below a given spatial scale, of order a hundred to a few hundred parsecs, cannot be resolved and must be treated by approximate, subresolution models. This includes, most importantly, the process of star formation, the detailed action of individual supernova events, the formation and growth of

[1] http://www.tng-project.org.

supermassive blackholes, and the near-field coupling of blackhole feedback energy to the surroundings. The updated TNG model for galaxy formation is described in [20, 21], and we employ it unchanged in all three flagship TNG simulations.[2]

The physical framework includes models of the most important physical processes for the formation and evolution of galaxies; (i) gas radiative microphysics, including primordial (H/He) and metal-line cooling and heating with an evolving ultraviolet/x-ray background field, (ii) star formation in dense interstellar medium (ISM) gas, (iii) the evolution of stellar populations and chemical enrichment, tracking supernovae Ia, II, and AGB stars, and individual species: H, He, C, N, O, Ne, Mg, Si, and Fe, (iv) galactic-scale outflows launched by stellar feedback, (v) the formation, binary mergers, and gas accretion by supermassive blackholes, (vi) blackhole feedback, operating in a thermal mode at high accretion rates and a kinetic 'wind' mode at low accretion rates. Aspects (iv) and (vi) have been substantially revised in TNG, and we describe them each in more detail.

2.1.1 Galactic Winds

First, galactic-scale outflows generated by stellar feedback are modeled using a kinetic wind approach [22], where the energy available from Type II (core-collapse) supernovae is used to stochastically kick star-forming gas cells away from galaxies. Winds particles are hydrodynamically decoupled from surrounding gas until they exit the dense, star-forming environment, which avoids small-scale interactions which cannot be modeled at the available resolution. The velocity of this wind-phase gas at injection is $v_{\rm w} \propto \sigma_{\rm DM}$ where $\sigma_{\rm DM}$ is the local one-dimensional dark matter velocity dispersion, with a minimum launch speed of $v_{\rm w,min} = 350$ km/s enforced. The mass loading of the winds, $\eta = \dot{M}_{\rm w}/\dot{M_{\rm SFR}}$ is then given by $\eta = 2(1 - \tau_{\rm w})e_{\rm w}/v_{\rm w}^2$ where $\tau_{\rm w} = 0.1$ is a fraction of energy chosen to be thermal, and $e_{\rm w}$ is a metallicity dependent factor which modifies the canonical 10^{51} erg available per event. As a result, the total energy available for these outflows scales with the star formation rate as $\Delta E = e_{\rm w}\dot{M}_{\rm SFR} \simeq 10^{41} - 10^{42}$ erg/s $\dot{M}_{\rm SFR}/(M_\odot/{\rm yr})$, depending on the local gas metallicity [full details in 21].

2.1.2 Black Hole Feedback

The second major change in TNG is blackhole feedback. Blackholes are formed in DM halos above a mass threshold, and are then able to accrete nearby gas at the Bondi rate, limited to the Eddington accretion rate. This accretion rate then determines their feedback mode. If the Eddington ratio exceeds a value of $\chi = \min[0.002({\rm M_{BH}}/10^8{\rm M}_\odot)^2, 0.1]$ we inject thermal energy (continuously) into the

[2] We also keep fixed all the relevant physical and numerical parameters when varying the numerical resolution, an approach not always adopted in computational galaxy formation. This allows us to establish a well-posed numerical problem towards which we can demonstrate convergence.

surrounding gas. The energy injection rate is $\Delta E_{\rm high} = \varepsilon_{\rm f,high}\varepsilon_{\rm r}\dot{M}_{\rm BH}c^2$ where $\varepsilon_{\rm f,high}$ is a coupling efficiency parameter in this 'high accretion state', and $\varepsilon_{\rm r}$ is the usual radiative accretion efficiency. Together, $\varepsilon_{\rm f,high}\varepsilon_{\rm r} = 0.02$, i.e. the net efficiency in this mode is about one percent. Below this accretion rate threshold, we instead inject kinetic energy (time-pulsed), in the form of an oriented, high-velocity wind which has a direction which changes between each event. Here the energy injection rate is $\Delta E_{\rm low} = \varepsilon_{\rm f,low}\dot{M}_{\rm BH}c^2$ with $\varepsilon_{\rm f,low} \leq 0.2$, the efficiency modulated as a function of environmental density [full details in 20].

This new, kinetic wind feedback from blackholes successfully terminates star formation in massive galaxies, transforming them from 'blue' disk-like systems similar to our own Milky Way, into 'red and dead' elliptical or spheroidal quenched systems [16, 23]. This bimodality of observed galaxy properties, which is seen in their colors, star forming rates, and structural properties for example, is a critical challenge for galaxy formation models [24].

2.1.3 Model Confirmations Across Observables

Other encouraging investigations and positive comparisons of TNG galaxy properties with observational data include, for example, their stellar contents, spatial clustering, and magnetic properties [14, 15, 17], as well as galaxy sizes, metal contents, ionized oxygen abundances, blackhole properties, and dark matter contents [23, 25–29].[3] These successes of the first two TNG simulations (TNG100 and TNG300), motivated and supported an even more ambitious project.

2.2 New Physics and Numerical Improvements

The IllustrisTNG simulation suite is founded upon the Arepo code [30]. Arepo solves the coupled equations of self-gravity and ideal, continuum magnetohydrodynamics [MHD; 31, 32], the former computed with the Tree-PM approach and the latter employing a Godunov/finite-volume method with a spatial discretization based on an unstructured, moving, Voronoi tessellation. The scheme is quasi-Lagrangian, second order in both space and time, and uses individual particle time-stepping.

The principle new physics that sets apart IllustrisTNG from previous numerical campaigns is the addition of magnetic fields. We have successfully implemented a method for the solution of the ideal MHD equations, using an 8-wave Powell cleaning scheme to maintain the zero divergence constraint [31, 32]. We have demonstrated the fidelity of this approach on both idealized test cases as well as galaxy simulations [33]. Since its original implementation, we have also made improvements to the MHD solver, through an additional timestep criterion which limits the magnitude of the source term applied for divergence cleaning.

[3] See http://www.tng-project.org/results/ for an ongoing publication list.

The AREPO code has been designed to efficiently execute large, parallel astrophysical simulations—the TNG50 simulation reviewed here is run on 16320 cores. At these scales there are several challenges, particularly given the highly coupled, high dynamic range of the galaxy formation problem. The TNG50 simulation itself captures a spatial dynamic range of $\sim 10^7$; the time hierarchy similarly requires evolution on timescales which differ by ten thousand or more. The previous MUSCL-Hancock time integration scheme has been replaced with a approach following Heun's method, a second-order Runge-Kutta variant which exhibits significantly better convergence properties [34]. The method for obtaining linear gradients of primitive fluid quantities has also been replaced with an iterative least-squares method, improving the convergence properties of the code as well as the conservation of angular momentum.

Finally, the long-range gravity FFT calculation now uses a new, column-based MPI-parallel FFT which improves scaling at high core numbers. Furthermore, the gravity calculation has been rewritten using a decomposition based on a recursive splitting of the N-body Hamiltonian into short- and long- timescale particle systems, such that the forces required to integrate the rapidly evolving particles can be computed with improved parallel efficiency, and in a mathematically robust way without any untreated coupling terms.

2.3 *Project Scope*

TNG50 is the third and final volume of the IllustrisTNG project. This simulation occupies a unique combination of large volume and high resolution—its details and numerical properties are given in Table 1 in comparison to the TNG series as a whole, while Fig. 1 gives a visual comparison of the volumes. Our 50 Mpc box is sampled by 2160^3 dark matter particles (with masses of $4 \times 10^5\,\mathrm{M}_\odot$) and 2160^3 initial gas cells (with masses of $8 \times 10^4\,\mathrm{M}_\odot$). The total number of resolution elements is therefore slightly over 20 billion. The *average* spatial resolution of star-forming interstellar medium (ISM) gas is $\sim$90 ($\sim$140) parsecs at $z = 1$ ($z = 6$). TNG50 has 2.5 times better spatial resolution, and 15 times better mass resolution, than TNG100 (or equivalently, original Illustris). This resolution approaches or exceeds that of modern 'zoom' simulations of individual galaxies [35, 36], while the volume contains $\sim$20,000 resolved galaxies with $M_\star > 10^7\,\mathrm{M}_\odot$ (at $z = 1$).

Table 1 Details of the TNG50 simulation in comparison to its two larger volume counterparts

Run name	Volume	N_{GAS}	N_{DM}	N_{TR}	m_{baryon}	m_{DM}	$\varepsilon_{\mathrm{gas,min}}$	$\varepsilon_{\mathrm{DM,stars}}$
	(Mpc^3)	–	–	–	($\mathrm{M}_\odot$)	($\mathrm{M}_\odot$)	(pc)	(pc)
TNG50	$\mathbf{51.7^3}$	$\mathbf{2160^3}$	$\mathbf{2160^3}$	$\mathbf{2160^3}$	$\mathbf{8.5 \times 10^4}$	$\mathbf{4.5 \times 10^5}$	**74**	**288**
TNG100	110.7^3	1820^3	1820^3	2×1820^3	1.4×10^6	7.5×10^6	185	740
TNG300	302.6^3	2500^3	2500^3	2500^3	1.1×10^7	5.9×10^7	370	1480

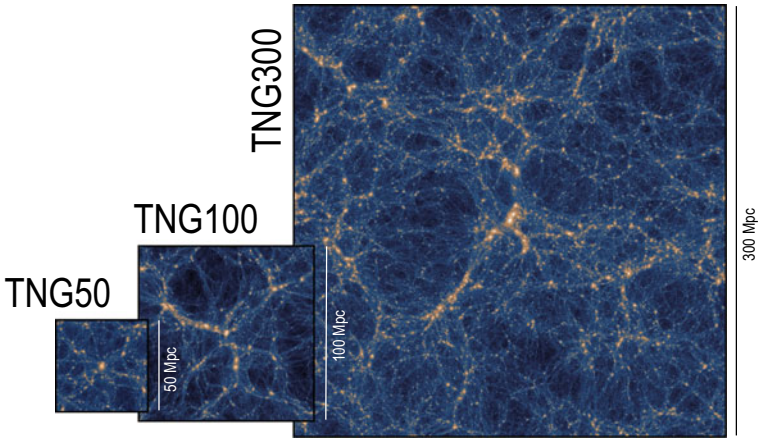

Fig. 1 Comparison of the TNG50 simulation to its larger volume counterparts. Due to the significantly higher resolution, the TNG50 run is by far the most computationally challenging of the three, and offers a unique configuration for a cosmological simulation

At the time of writing, the TNG50 simulation has been evolved from the initial conditions of the Universe to $z \sim 0.6$ (8 billion years after), and we are currently completing the run to reach the current epoch of cosmic evolution ($z = 0$).

TNG50 contains roughly 100 Milky Way mass-analogs, enabling detailed comparisons to our own galaxy at $z = 0$. It also hosts one massive galaxy cluster with a total mass $\sim 10^{14}\,\mathrm{M}_\odot$, a Virgo-like analog, and dozens of group sized halos at $\sim 10^{13}\,\mathrm{M}_\odot$. All of these massive objects are simulated at higher numerical resolution than in any previously published study, enabling studies not only of the gaseous halos and central galaxies, but also of the large populations of their satellite galaxies.

3 The TNG50 Simulation: Early Results

We proceed to show selected early results from TNG50, focusing on the internal structural properties of the gaseous components of galaxies and their halos, topics which are explored in a number of papers currently in preparation. We can now analyze a fully representative, simulated galaxy population spanning $10^7 < M_\star/\mathrm{M}_\odot < 10^{11.5}$ across intermediate to high redshifts, $1 < z < 8$. The high resolution of TNG50 is specifically exploited to investigate scales, regimes, and scientific questions not addressable using the other two TNG simulations.

This coverage in redshift range and galaxy stellar mass enables us to make quantitative predictions for signatures observable with the James Webb Space Telescope (JWST), now anticipated to launch in 2019, as well as recent

ground-based IFU instruments such as MUSE, SINFONI, and KCWI. The key science drivers of TNG50 focus not only on the present day ($z = 0$), but also at earlier epochs, from cosmic noon ($z \sim 2$) through reionization ($z \sim 6$).

3.1 Resolving Galactic Structure

The internal structures of the progenitors of present-day galaxies are observed at $z \sim 2$ from ground based telescopes using adaptive-optics techniques, which enable kiloparsec scale structure by tracing bright emission lines from hydrogen (such as Hα) or metals (i.e. OIII), as in [37]. Using TNG50 we can provide model predictions for projected radial profiles and resolved 2D maps of gas density, star formation rate (Hα), gas-phase metallicity, and gas line-of-sight velocity dispersion.

In Fig. 2 we show nine examples of star-formation surface density of $z = 1$ massive galaxies. Quantitative measurements of the morphology of the star-forming gas, as will be traceable at high-redshift through rest-frame UV and optical nebular emission lines (e.g. MgII, FeII, OII, and OIII), discriminate between galaxy evolutionary stages. In general, star formation peaks towards the center of galaxies as it follows the local gas density according to the Schmidt-Kennicutt relation. Small scale structure at sub-kiloparsec scale is easily resolved by TNG50, revealing rich morphological features including flocculent spiral arms of extended, low-density gas as well as clumpy sub-structures. We see directly how outflows generated from the nuclear regions of disks leave signatures in the gas left behind, evidenced in the central depressions, which result from the direct expulsion of gas due to the action of the kinetic supermassive blackhole feedback.

Despite their strong ordered rotation, galactic disks at $z = 1$ are highly turbulent gaseous reservoirs. These settle with time: the peak velocity dispersion at $M_\star = 10^{10.5}\,\mathrm{M}_\odot$ drops from >400 km/s at $z = 6$ to ~100 km/s at $z = 1$. These trends, as a function of galaxy mass and cosmic time, can be directly tested against upcoming observational programs, providing a strong constraint on our galaxy formation model. At the same time, by constructing synthetic observations of, for example, the Hα emission from hydrogen atoms excited by nearby young stars, we can assess observational biases and aid in the robust interpretation of observational results which do not have access to the intrinsic properties of the galaxies.

3.2 Heavy Metal Distribution and Metallicity Gradients

Metallicity gradients—that is, radial variations in the enrichment of galaxies by heavy elements—have been observed in local $z = 0$ systems as part of the SDSS MANGA survey [38], but not yet at higher redshifts. Within the framework of inside-out disk

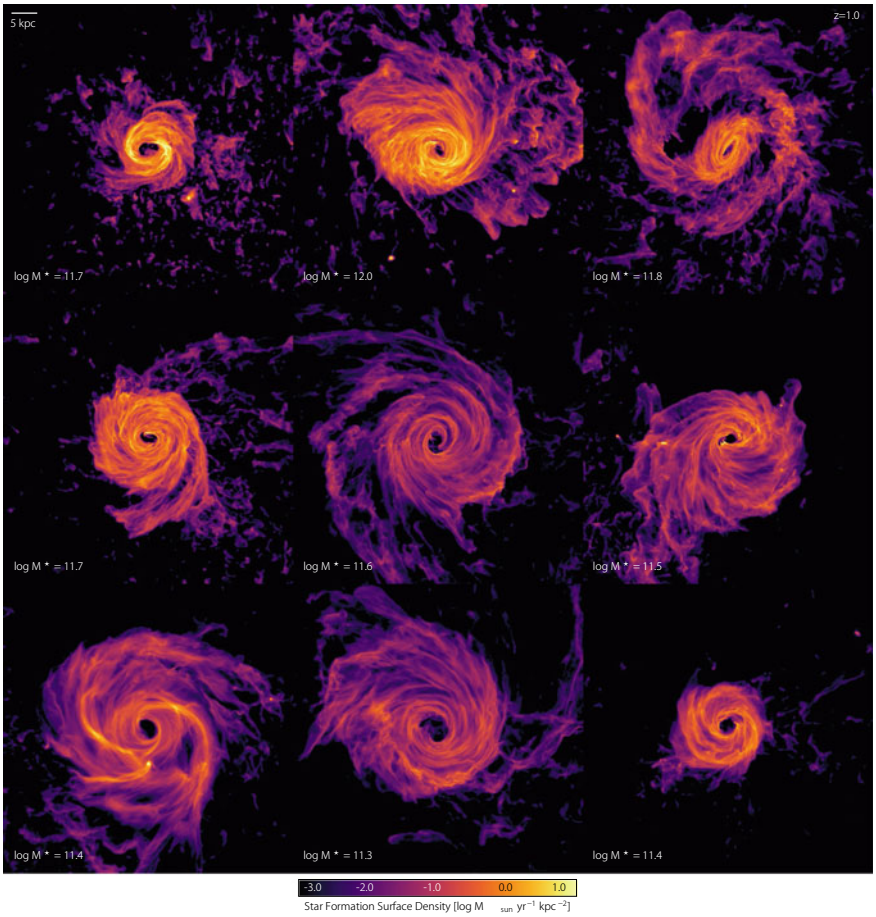

Fig. 2 Nine examples of massive galaxies at redshift one. Each is rotated so that it is viewed face-on, emphasizing the spiral structure of disk-like galaxies. Here we show projections of the star formation rate surface density, in units of $M_\odot\ yr^{-1}\ kpc^{-2}$. Star formation activity increases towards the centers, following the gas density, while fine-grained structure on hundred parsec scales is able to develop as a result of the high gas spatial resolution in TNG50

growth, metallicities in central regions of massive galaxies versus their outskirts reflects an equilibrium between ongoing stellar nucleosynthesis, supernova feedback and gas inflows. That is, they encode the relation between chemical enrichment from stars and ejective outflows due to feedback on local scales.

In Fig. 3 we show average metallicity profiles, stacking many galaxies at $z \sim 0.7$ together at each mass (different colored lines), as a function of radius. Metallicities monotonically increase with mass, while the extended gradients of the stacked profiles gradually flatten. At some point a critical threshold is reached at $M_\star \simeq 10^{11}$ $M_\odot$, above which the central profiles become constant with distance within <10 kpc.

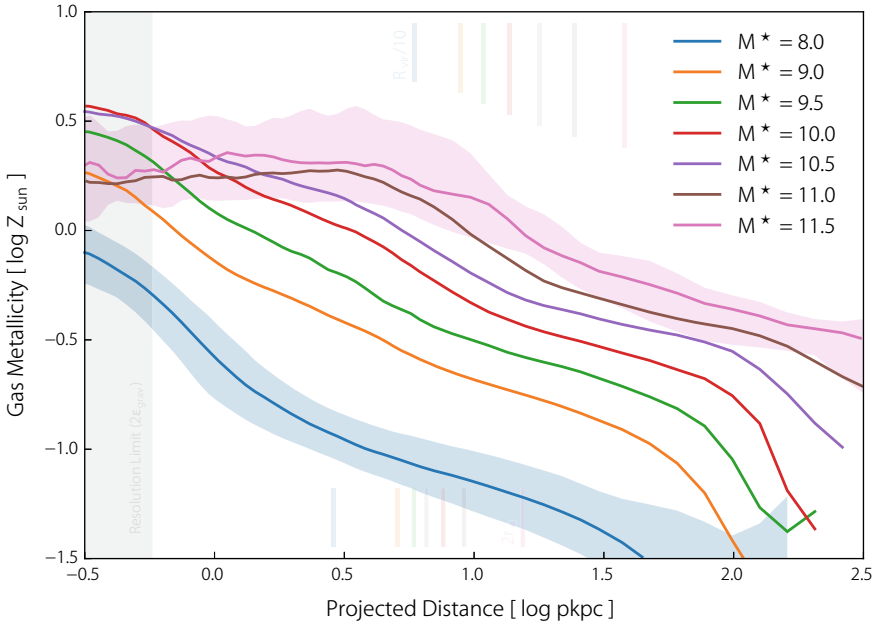

Fig. 3 Median radial profiles of gas-phase metallicity—that is, the relative enrichment of gas by elements heavier than helium as a function of distance from the galaxy center. Shown in 2D projection, as would be observed, where each colored line represents a stack of all galaxies with approximately the stellar mass $M_\star$ as indicated in the legend. Each stack contains between a few, and a few thousand, galaxies. Metallicities generally increase with mass, while the gradients encode a wealth of information on the interplay between gas-poor inflows and gas-rich outflows

This complete flattening of metallicity gradients is due to post-outflow, metal-poor inflows, and corresponds to an inversion of the central gradient of star formation rate. Whether these gas inflows arise from cooling out of the gaseous halo atmosphere, primordial cosmological accretion, or radial flux through the disk due to angular momentum loss processes remains to be investigated.

At higher redshifts (not shown), we also see that galaxies as small as $10^8\,\mathrm{M}_\odot$ reach solar metallicity in their centers already at $z = 6$, although this value drops quickly to $Z_\odot/10$ at $\sim$10 kpc as a result of a nearly time-invariant metallicity gradient for galaxies of a given mass, which is place already by $z = 6$ and supported by a pre-enriched cosmological inflow. This early distribution of metals into low-density environments occurs as a result of high velocity outflows driven by the blackhole winds, leading to large-distance pollution of the circumgalactic and intergalactic medium (IGM) by metal-enriched gas at high redshift.

3.3 Gas-Dynamical Processes in the Intracluster Medium (ICM)

The thermodynamical state of the intracluster medium of galaxy clusters is a sensitive probe of galaxy formation physics, plasma physics, and even cosmology. Observations at X-ray and radio wavelengths have revealed a rich level of detail, including sub-cluster components, ram pressure stripped tails of gas, and sharp jumps in the temperature and density of the gas resulting from bow shocks [39].

In Fig. 4 we show four different views of a single massive galaxy cluster in TNG50. Stars (upper left) trace individual galaxies, while the temperature distribution (upper right) peaking at over 100 million Kelvin in the halo center might lead one to conclude a rather homogeneous and uniform intra-cluster medium (ICM). In reality, this gaseous reservoir is highly dynamic and constantly being stirred up by the influence of baryonic feedback processes from the central galaxy and its many luminous satellites, as seen by the distribution and structure of hydrodynamical shocks (lower left) and leading to significant chemical enrichment of the cluster volume (lower right). We can quantify the energy dissipation rates and Mach numbers of shock fronts, which are typically mildly supersonic. The cooling properties of the hot halo gas are modulated not only by feedback from the central blackhole, but also by supernovae-driven winds launched by infalling satellite galaxies. The ICM is substantially enriched by iron produced by both supernovae type Ia and type II, and substantially so out to a significant fraction of the virial radius. This metal-rich gas has a turbulent velocity structure down to the smallest resolvable scales, which can influence the physical interpretation of high-resolution spectroscopic x-ray line observations [40].

The resolution of TNG50 also allows us to study cluster-member luminous satellites down to $\sim 10^7\,\mathrm{M}_\odot$, which will provide a detailed picture of the temporal evolution of such an ensemble of heirarchically accumulating galaxies.

3.4 Characteristic Sizes of Galaxies and Halos

The relationship between the size of a galaxy and the size (or mass) of its dark matter halo is fundamentally related to the theory of hierarchical assembly and collapse [41], while observations of galaxy sizes in different tracers—star-forming gas, optical stellar light, or molecular line emission, as examples—provide direct observational probes [42]. As TNG50 evolves all of the relevant baryonic components self-consistently together, we can provide direct predictions for the relationships between different 'sizes' of galaxies and halos, as shown in Fig. 5 at $z \simeq 0.7$. Here we compare, across five order of magnitude in stellar mass, the halo virial radius (green), the radius enclosing half the gaseous mass (blue), the radius enclosing half the stellar mass (orange), the optical 'effective radius' R_e (red), the half light radius of star-forming gas (purple), and the extent of neutral hydrogen (HI; brown).

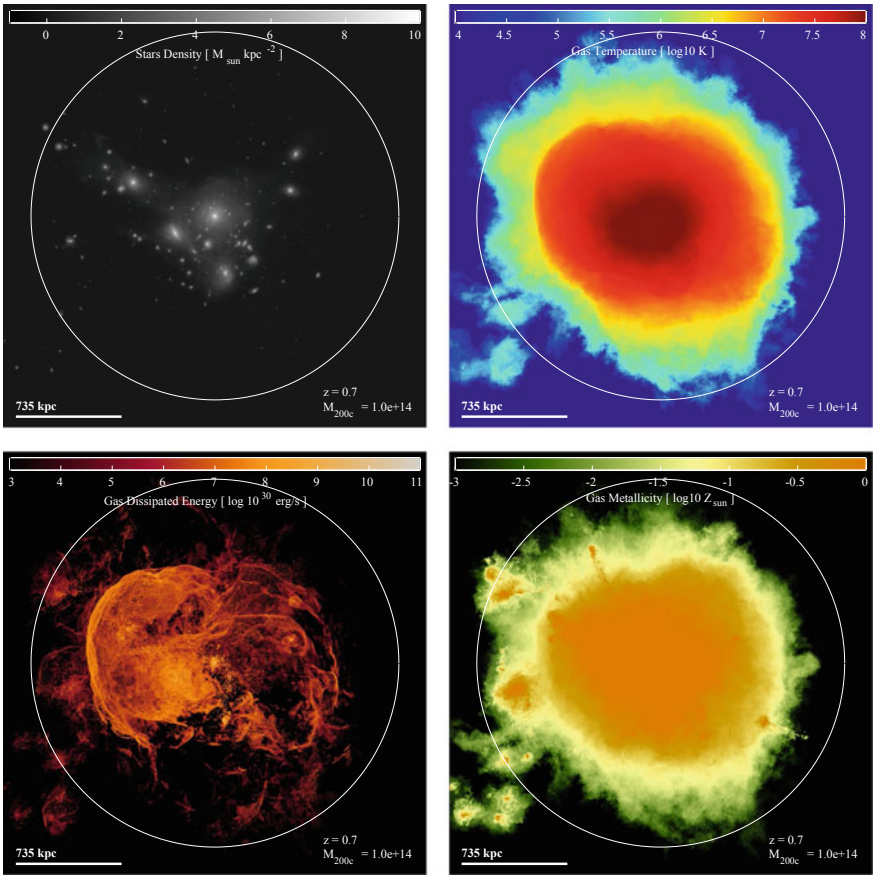

Fig. 4 Four different views of one of the most massive galaxy clusters in the TNG50 simulation at $z \simeq 0.7$. In each case, the circle demarcates the virial radius ($r_{200,\mathrm{crit}}$). We show: stellar mass (upper left), gas temperature (upper right), energy dissipation rate due to hydrodynamical shocks (lower left), and gas metallicity (lower right). Complex galaxy interactions are encoded in the small-scale features of the intracluster medium (ICM) gas, particularly in hydrodynamical shock structures

After the dark matter halo itself, the gas is the most extended component. This is followed by the neutral hydrogen component, which is more concentrated than the gas overall as it becomes ionized in low-density halo outskirts due to photoionization from the ultraviolet/x-ray background radiation field. Surprisingly, the predicted Hα emission is generally as concentrated as the optical light from the stellar component itself, although this breaks down at small (large) masses, where it is smaller (larger), respectively. At $M_\star \simeq 10^{10}\,\mathrm{M}_\odot$, the gas of a galactic halo extends to roughly an order of magnitude larger distances than its stars, but in quantitative detail this depends on the observational tracer used for both components. TNG50 provides details not only on the extent, but also the shape (e.g. axis ratios) and morphology (e.g. asymmetry)

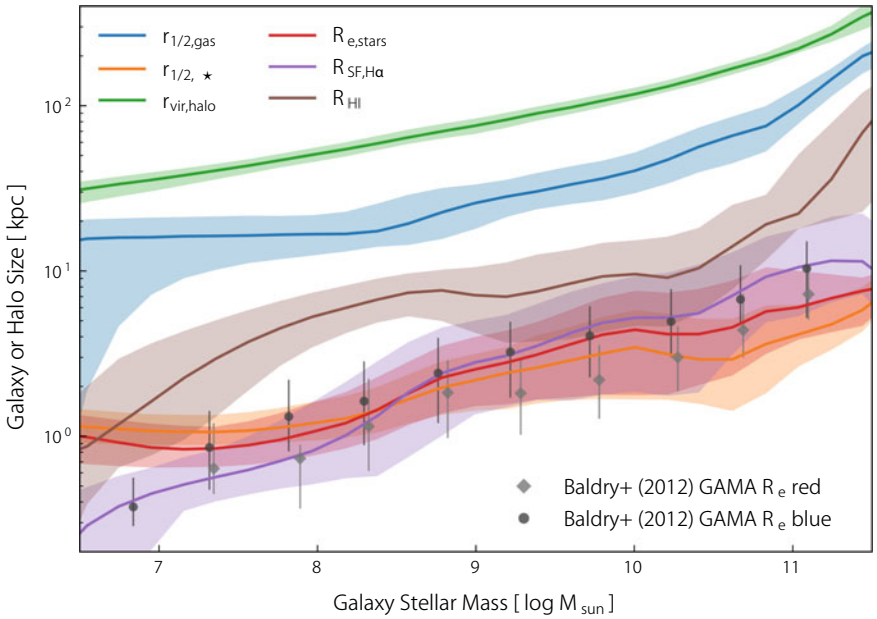

Fig. 5 Characteristic sizes of galaxies and galaxy halos as a function of stellar mass, in the TNG50 simulation at $z \simeq 0.7$. Increasing massive galaxies are always larger, and here we compare: the halo virial radius (green), the radii enclosing half the gaseous mass (blue) and half the stellar mass (orange), the optical 'effective radius' R_e in a putative observation with the F115W filter aboard the James Web Space Telescope (JWST; red), the Hα half light radius of star-forming gas (purple), and the neutral hydrogen (HI) size (brown). Observations from [43] at $z = 0$ are shown for reference

of each component. Although already well constrained at low redshift, these aspects of the galaxy population are largely unknown at earlier epochs and are a predictive regime for the current generation of cosmological simulations.

4 Conclusions

Despite the numerous theoretical achievements of recent large volume simulations such as Illustris, Eagle, or even TNG100 and TNG300, their limited mass and spatial resolution complicate any study of the structural details of galaxies less massive than a few times $10^9\,M_\odot$. In contrast, projects focused on 'zoom' simulations of one or a handful of galaxies are constrained by their small sample sizes and inability to construct cosmologically representative volumes for statistical population analyses. For the most massive galaxy clusters, simulations with sufficient resolution to simultaneously model the co-evolving population of satellite galaxies have been prohibited

by the large computational requirements as well as the complexity of the physical mechanisms which operate to shape the circumgalactic and intracluster gas.

TNG50 is already proving to be an instrumental theoretical tool for the comparison—via mock observations of the simulated data—with existing and upcoming observational datasets. These include, for example, the star formation histories and abundances of dwarf galaxies in the first few billion years of the history of the Universe (with HST, JWST); the detailed mapping of our Galaxy's stellar system (e.g. with Gaia-ESO, Rave, APOGEE, GALAH, SEGUE, DES); the imaging and spectroscopic characterization of the galaxy populations residing in nearby galaxy clusters like Virgo, Fornax, and Coma (SAURON, ATLAS-3D, NGVS); the X-ray maps of the outskirts of galaxy clusters with the SUZAKU telescope; integral-field spectroscopy campaigns of nearby galaxies (MANGA, CALIFA); the characterization of circumgalactic and IGM gas (e.g. COS-Halo); and magnetic field measurements in halos (LOFAR, SKA) and in the disks of galaxies (ASKAP). In each case, TNG50 will be able to provide a foundation for theoretical interpretation.

The IllustrisTNG project aims to redefine the state-of-the-art of cosmological hydrodynamical simulations of galaxy formation. Even beyond our immediate scientific investigations, the TNG50 simulation will be a unique platform to pursue as of yet unimagined future projects, as we are now able to treat cosmological simulations as almost open ended laboratories for studying galaxy formation physics.

Acknowledgements The authors acknowledge the Gauss Centre for Supercomputing (GCS) for providing computing time for the GCS Large-Scale Projects GCS-ILLU (2014) and GCS-DWAR (2016) on the GCS share of the supercomputer Hazel Hen at the High Performance Computing Center Stuttgart (HLRS). DN acknowledges additional simulations and analysis carried out on supercomputers at the Max Planck Computing and Data Facility (MPCDF, formerly known as RZG). VS, RW, and RP acknowledge support through the European Research Council under ERC-StG grant EXAGAL-308037 and would like to thank the Klaus Tschira Foundation.

References

1. C.S. Frenk, S.D.M. White, M. Davis, ApJ **271**, 417 (1983). https://doi.org/10.1086/161209
2. M. Davis, G. Efstathiou, C.S. Frenk, S.D.M. White, ApJ **292**, 371 (1985). https://doi.org/10.1086/163168
3. J.F. Navarro, C.S. Frenk, S.D.M. White, ApJ **490**, 493 (1997). https://doi.org/10.1086/304888
4. A.E. Evrard, T.J. MacFarland, H.M.P. Couchman, J.M. Colberg, N. Yoshida, S.D.M. White, A. Jenkins, C.S. Frenk, F.R. Pearce, J.A. Peacock, P.A. Thomas, ApJ **573**, 7 (2002). https://doi.org/10.1086/340551
5. V. Springel, S.D.M. White, A. Jenkins, C.S. Frenk, N. Yoshida, L. Gao, J. Navarro, R. Thacker, D. Croton, J. Helly, J.A. Peacock, S. Cole, P. Thomas, H. Couchman, A. Evrard, J. Colberg, F. Pearce, Nature **435**, 629 (2005). https://doi.org/10.1038/nature03597
6. M. Vogelsberger, S. Genel, V. Springel, P. Torrey, D. Sijacki, D. Xu, G. Snyder, D. Nelson, L. Hernquist, MNRAS **444**, 1518 (2014). https://doi.org/10.1093/MNRAS/stu1536
7. M. Vogelsberger, S. Genel, V. Springel, P. Torrey, D. Sijacki, D. Xu, G. Snyder, S. Bird, D. Nelson, L. Hernquist, Nature **509**, 177 (2014). https://doi.org/10.1038/nature13316
8. S. Genel, M. Vogelsberger, V. Springel, D. Sijacki, D. Nelson, G. Snyder, V. Rodriguez-Gomez, P. Torrey, L. Hernquist, MNRAS **445**, 175 (2014). https://doi.org/10.1093/mnras/stu1654

9. D. Sijacki, M. Vogelsberger, S. Genel, V. Springel, P. Torrey, G.F. Snyder, D. Nelson, L. Hernquist, MNRAS **452**, 575 (2015). https://doi.org/10.1093/mnras/stv1340
10. J. Schaye, R.A. Crain, R.G. Bower, M. Furlong, M. Schaller, T. Theuns, C. Dalla Vecchia, C.S. Frenk, I.G. McCarthy, J.C. Helly, A. Jenkins, Y.M. Rosas-Guevara, S.D.M. White, M. Baes, C.M. Booth, P. Camps, J.F. Navarro, Y. Qu, A. Rahmati, T. Sawala, P.A. Thomas, J. Trayford, MNRAS **446**, 521 (2015). https://doi.org/10.1093/mnras/stu2058
11. R.A. Crain, J. Schaye, R.G. Bower, M. Furlong, M. Schaller, T. Theuns, C. Dalla Vecchia, C.S. Frenk, I.G. McCarthy, J.C. Helly, A. Jenkins, Y.M. Rosas-Guevara, S.D.M. White, J.W. Trayford, MNRAS **450**, 1937 (2015). https://doi.org/10.1093/mnras/stv725
12. Y. Dubois, S. Peirani, C. Pichon, J. Devriendt, R. Gavazzi, C. Welker, M. Volonteri, MNRAS **463**, 3948 (2016). https://doi.org/10.1093/mnras/stw2265
13. K. Dolag, E. Komatsu, R. Sunyaev, MNRAS **463**, 1797 (2016). https://doi.org/10.1093/mnras/stw2035
14. A. Pillepich, D. Nelson, L. Hernquist, V. Springel, R. Pakmor, P. Torrey, R. Weinberger, S. Genel, J.P. Naiman, F. Marinacci, M. Vogelsberger, MNRAS **475**, 648 (2018). https://doi.org/10.1093/mnras/stx3112
15. V. Springel, R. Pakmor, A. Pillepich, R. Weinberger, D. Nelson, L. Hernquist, M. Vogelsberger, S. Genel, P. Torrey, F. Marinacci, J. Naiman, MNRAS **475**, 676 (2018). https://doi.org/10.1093/mnras/stx3304
16. D. Nelson, A. Pillepich, V. Springel, R. Weinberger, L. Hernquist, R. Pakmor, S. Genel, P. Torrey, M. Vogelsberger, G. Kauffmann, F. Marinacci, J. Naiman, MNRAS **475**, 624 (2018). https://doi.org/10.1093/mnras/stx3040
17. F. Marinacci, M. Vogelsberger, R. Pakmor, P. Torrey, V. Springel, L. Hernquist, D. Nelson, R. Weinberger, A. Pillepich, J. Naiman, S. Genel, ArXiv e-prints (2017)
18. J.P. Naiman, A. Pillepich, V. Springel, E. Ramirez-Ruiz, P. Torrey, M. Vogelsberger, R. Pakmor, D. Nelson, F. Marinacci, L. Hernquist, R. Weinberger, S. Genel, ArXiv e-prints (2017)
19. D. Nelson, A. Pillepich, S. Genel, M. Vogelsberger, V. Springel, P. Torrey, V. Rodriguez-Gomez, D. Sijacki, G.F. Snyder, B. Griffen, F. Marinacci, L. Blecha, L. Sales, D. Xu, L. Hernquist, Astron. Comput. **13**, 12 (2015). https://doi.org/10.1016/j.ascom.2015.09.003
20. R. Weinberger, V. Springel, L. Hernquist, A. Pillepich, F. Marinacci, R. Pakmor, D. Nelson, S. Genel, M. Vogelsberger, J. Naiman, P. Torrey, MNRAS **465**, 3291 (2017). https://doi.org/10.1093/mnras/stw2944
21. A. Pillepich, V. Springel, D. Nelson, S. Genel, J. Naiman, R. Pakmor, L. Hernquist, P. Torrey, M. Vogelsberger, R. Weinberger, F. Marinacci, MNRAS **473**, 4077 (2018). https://doi.org/10.1093/mnras/stx2656
22. V. Springel, L. Hernquist, MNRAS **339**, 289 (2003). https://doi.org/10.1046/j.1365-8711.2003.06206.x
23. R. Weinberger, V. Springel, R. Pakmor, D. Nelson, S. Genel, A. Pillepich, M. Vogelsberger, F. Marinacci, J. Naiman, P. Torrey, L. Hernquist, ArXiv e-prints (2018)
24. S. Cole, C.G. Lacey, C.M. Baugh, C.S. Frenk, MNRAS **319**, 168 (2000). https://doi.org/10.1046/j.1365-8711.2000.03879.x
25. D. Nelson, G. Kauffmann, A. Pillepich, S. Genel, V. Springel, R. Pakmor, L. Hernquist, R. Weinberger, P. Torrey, M. Vogelsberger, F. Marinacci, MNRAS (2018). https://doi.org/10.1093/mnras/sty656
26. P. Torrey, M. Vogelsberger, F. Marinacci, R. Pakmor, V. Springel, D. Nelson, J. Naiman, A. Pillepich, S. Genel, R. Weinberger, L. Hernquist, ArXiv e-prints (2017)
27. S. Genel, D. Nelson, A. Pillepich, V. Springel, R. Pakmor, R. Weinberger, L. Hernquist, J. Naiman, M. Vogelsberger, F. Marinacci, P. Torrey, MNRAS **474**, 3976 (2018). https://doi.org/10.1093/mnras/stx3078
28. M. Vogelsberger, F. Marinacci, P. Torrey, S. Genel, V. Springel, R. Weinberger, R. Pakmor, L. Hernquist, J. Naiman, A. Pillepich, D. Nelson, MNRAS **474**, 2073 (2018). https://doi.org/10.1093/mnras/stx2955
29. M.R. Lovell, A. Pillepich, S. Genel, D. Nelson, V. Springel, R. Pakmor, F. Marinacci, R. Weinberger, P. Torrey, M. Vogelsberger, L. Hernquist, ArXiv e-prints (2018)

30. V. Springel, MNRAS **401**, 791 (2010). https://doi.org/10.1111/j.1365-2966.2009.15715.x
31. R. Pakmor, A. Bauer, V. Springel, MNRAS **418**, 1392 (2011). https://doi.org/10.1111/j.1365-2966.2011.19591.x
32. R. Pakmor, V. Springel, MNRAS **432**, 176 (2013). https://doi.org/10.1093/mnras/stt428
33. R. Pakmor, F. Marinacci, V. Springel, ApJL **783**, L20 (2014). https://doi.org/10.1088/2041-8205/783/1/L20
34. R. Pakmor, V. Springel, A. Bauer, P. Mocz, D.J. Munoz, S.T. Ohlmann, K. Schaal, C. Zhu, MNRAS **455**, 1134 (2016). https://doi.org/10.1093/mnras/stv2380
35. R.J.J. Grand, F.A. Gómez, F. Marinacci, R. Pakmor, V. Springel, D.J.R. Campbell, C.S. Frenk, A. Jenkins, S.D.M. White, ArXiv e-prints (2016)
36. P.F. Hopkins, A. Wetzel, D. Keres, C.A. Faucher-Giguere, E. Quataert, M. Boylan-Kolchin, N. Murray, C.C. Hayward, S. Garrison-Kimmel, C. Hummels, R. Feldmann, P. Torrey, X. Ma, D. Angles-Alcazar, K.Y. Su, M. Orr, D. Schmitz, I. Escala, R. Sanderson, M.Y. Grudic, Z. Hafen, J.H. Kim, A. Fitts, J.S. Bullock, C. Wheeler, T.K. Chan, O.D. Elbert, D. Narananan, ArXiv e-prints (2017)
37. N.M. Förster Schreiber, A. Renzini, C. Mancini, R. Genzel, N. Bouché, G. Cresci, E.K.S. Hicks, S.J. Lilly, Y. Peng, A. Burkert, C.M. Carollo, A. Cimatti, E. Daddi, R.I. Davies, S. Genel, J.D. Kurk, P. Lang, D. Lutz, V. Mainieri, H.J. McCracken, M. Mignoli, T. Naab, P. Oesch, L. Pozzetti, M. Scodeggio, K. Shapiro Griffin, A.E. Shapley, A. Sternberg, S. Tacchella, L.J. Tacconi, S. Wuyts, G. Zamorani, ArXiv e-prints (2018)
38. F. Belfiore, R. Maiolino, C. Tremonti, S.F. Sánchez, K. Bundy, M. Bershady, K. Westfall, L. Lin, N. Drory, M. Boquien, D. Thomas, J. Brinkmann, MNRAS **469**, 151 (2017). https://doi.org/10.1093/mnras/stx789
39. H.R. Russell, J.S. Sanders, A.C. Fabian, S.A. Baum, M. Donahue, A.C. Edge, B.R. McNamara, C.P. O'Dea, MNRAS **406**, 1721 (2010). https://doi.org/10.1111/j.1365-2966.2010.16822.x
40. Hitomi Collaboration, Nature **535**, 117 (2016). https://doi.org/10.1038/nature18627
41. H.J. Mo, S. Mao, S.D.M. White, MNRAS **295**, 319 (1998). https://doi.org/10.1046/j.1365-8711.1998.01227.x
42. R.S. Somerville, P. Behroozi, V. Pandya, A. Dekel, S.M. Faber, A. Fontana, A.M. Koekemoer, D.C. Koo, P.G. Pérez-González, J.R. Primack, P. Santini, E.N. Taylor, A. van der Wel, MNRAS **473**, 2714 (2018). https://doi.org/10.1093/mnras/stx2040
43. I.K. Baldry, S.P. Driver, J. Loveday, E.N. Taylor, L.S. Kelvin, J. Liske, P. Norberg, A.S.G. Robotham, S. Brough, A.M. Hopkins, S.P. Bamford, J.A. Peacock, J. Bland-Hawthorn, C.J. Conselice, S.M. Croom, D.H. Jones, H.R. Parkinson, C.C. Popescu, M. Prescott, R.G. Sharp, R.J. Tuffs, MNRAS **421**, 621 (2012). https://doi.org/10.1111/j.1365-2966.2012.20340.x

44065 HypeBBH Yearly Report—High Performance Computing Services at HLRS

Federico Guercilena, Elias Most and Luciano Rezzolla

1 Introduction

The allocation "44065 HypeBBHs" on the system CRAY XC40 (HAZEL HEN) at HLRS has been awarded to our research group in February 2015 for one year, then extended in February 2016 until December 2016, becoming one of the main computing resources available to us. A request for a further extension until December 2017 and new resources allocation has been submitted, and we have been granted access to the machine with full approval of our application.

The scientific research carried on in the group relates to a number of broad topics in the field of general relativistic astrophysics. These topics, which fall in general under the label of "physics of compact objects", include:

- the general behaviour of black hole systems in vacuum
- the study of rigidly and differentially rotating isolated neutron stars
- the evolution of neutron stars and accretion disks systems
- the evolution and properties of magnetized neutron stars in the contexts of both ideal and resistive magnetohydrodynamics
- the study of ejecta in binary neutron star systems and the resulting implications for nucleosynthesis.

Due to the sheer complexity of the physical models involved in this field of research, no realistic analytical solutions are available. The main tools of our research are therefore large scale numerical simulations of the physical system of interest. As such another important line of research we follow is the development of better numerical methods to improve the accuracy and/or performance of our results. This state of affairs in turn makes computing resources such as the ones provided by HLRS a very important asset to us.

F. Guercilena · E. Most · L. Rezzolla (✉)
Institute for Theoretical Physics (ITP), Goethe University, Max-von-Laue-Str. 1, 60438 Frankfurt, Germany
e-mail: rezzolla@th.physik.uni-frankfurt.de

W. E. Nagel et al. (eds.), *High Performance Computing in Science and Engineering '18*, https://doi.org/10.1007/978-3-030-13325-2_2

2 Numerical Methods

Our simulations are performed using several codes developed by members of the group and others publicly available as part of the `Einstein Toolkit` suite [1–3], of which some of the members of our group are developers and/or contributors.

We rely on the Einstein Toolkit as the main infrastructure for all our simulations, in particular to handle the set up of the numerical grid and mesh refinement, the time evolution of fields (in a method-of-lines fashion using Runge-Kutta integrators), the output, checkpointing, memory access and management.

We discretize the Einstein equations for the spacetime evolution using a standard finite-difference (e.g., [4]) method where all the derivatives, with the exception of the terms associated with the advection along the shift vector, for which we use a stencil upwinded by one grid point, are computed with a centered stencil. Typically all these terms are computed with an eighth-order accurate scheme in vacuum and fourth-order in the presence of matter. To ensure the nonlinear stability of the scheme we add a ninth-order (fifth-order respectively) Kreiss-Oliger [5] style artificial dissipation.

Specifically, we use the publicly available finite-difference `McLachlan` code [6], which uses the so-called BSSN [7–9] or CCZ4 [10] formulations of Einstein's equations solved by high order finite-differencing. It contains state-of-the art gauge conditions and supports OpenMP-parallelization and explicit instruction vectorisation. `McLachlan` is freely available under the GPL. It makes use of the `Kranc` framework [11, 12] to automatically generate optimized, robust C++ code from Mathematica formulas describing the partial differential equations. More recently we have developed a new framework to automatically generate lengthy tensor expressions using modern compile-time evaluated C++ 14 expression templates. Using this framework we have not only reimplemented the BSSN, CCZ4 and Z4c [13] equations, but also managed to a get a significant speed-up compared to the previous `McLachlan` implementation.

To discretize the equations of hydrodynamics and magnetohydrodynamics and couple them to the evolution of the spacetime, we employ the `WhiskyTHC`, `WhiskyMHD` and `WhiskyResistive` codes. These are proprietary codes mainly developed in our group. They provide finite-difference and finite-volume based discretizations of the Euler and Maxwell-Euler equations along with state-of-the-art algorithms (such as high-order reconstruction methods, Riemann solvers and flux limiters) to handle the difficulties arising in the solutions of such equations.

The `WhiskyTHC` [14–16] code in particular also includes algorithms which allow the inclusion of realistic microphysical processes in the hydrodynamical simulations, such as realistic equations of state and neutrino leakage schemes.

Additionally we make use of the recently developed `FIL` code that is a high-order extension of the publically available `IllinoisGRMHD` code [17]. More specifically, it evolves the staggered vector potential using the upwind constraint transport method to preserve the divergence constraint on the magnetic field. It also uses a fourth-order accurate WENO flux update and includes support for currently used temperature

dependent equations of state and neutrino leakage and can be coupled to an M0 neutrino absorption scheme.

These evolution codes were developed in the context of the `Cactus` framework [18, 19], a framework providing MPI parallelization, data management and an API to bind together different modules written in different computer languages, which is distributed under GPL 2.0.

All the codes are internally OpenMP-parallelized, leading to a very efficient hybrid OpenMP/MPI parallelization model. The use of mesh-refinement techniques is of fundamental importance in our simulations. For this reason, we use the `Carpet` driver [20] that implements a vertex- or cell-centered adaptive-mesh-refinement scheme adopting nested and moving grids. This enables the code to follow the moving compact objects (black holes or neutron stars) with fine-resolution grids, while covering with coarser grids a much larger volume needed for the accurate treatment of the gravitational waves.

3 Job Statistics and Resources Usage

The typical job size for our projects is largely dependent on the type of physical system we are modelling, the microphysical processes involved and of course the level of accuracy needed, which sets constraints on numerical parameters such as the resolution, domain size and order of the method. Nonetheless we can provide some estimates. A typical job can require the use of 50 nodes (1200 cores) for a period of 24 ours at low resolution and twice as much (100 nodes/2400 cores) for several days at mid-high resolution. In the hybrid MPI/OpenMP parallelization scheme that we employ, this results in a total of 50–100 MPI processes (2 per node), each of them spawning 12 threads each. We normally do not exploit hyperthreading and attempt to bind each thread to a separate physical core.

A grand total of 15,808,872 core-hours was awarded to us, and we have exhausted it, with a usage of 99.97% as of 06/04/2018. At present 14 researchers within our group have access to computing resources at HLRS, but of these 4 none are actually active, as we have currently taken to completion all projects on this platform.

4 Completed Projects and Publications

4.1 Entropy-Limited Hydrodynamics: A Novel Approach to Relativistic Hydrodynamics

We developed a new approach for the computation of numerical fluxes arising in the discretization of hyperbolic equations in conservation form, which we call ELH: entropy-limited hydrodynamics. ELH is based on the hybridisation of an unfiltered